17th World Conference on Earthquake Engineering, 17WCEE

Sendai, Japan - September 27th to October 2nd, 2021

THE INFLUENCE OF ROTATIONAL COMPONENTS OF EARTHQUAKE GROUND MOTIONS ON BUILDING RESPONSE

S. Wu[1], E. Eckert[2], J. Huang[3], D. McCallen[4]

[1] *Postdoctoral scholar, Department of Civil and Environmental Engineering, University of Nevada, Reno, Reno, NV, 89557, suiwenw@unr.edu*
[2] *Research assistant, Energy Geosciences Division, Lawrence Berkeley National Laboratory, Berkeley, CA, 94720, eeckert@nevada.unr.edu*
[3] *Research assistant, Department of Civil and Environmental Engineering, University of Nevada, Reno, Reno, NV, 89557, jfhuang@nevada.unr.edu*
[4] *Professor and Director of the Center for Civil Engineering Earthquake Research, University of Nevada, Reno, NV, 89557, and Senior Scientist, Lawrence Berkeley National Laboratory, dmccallen@unr.edu*

Abstract

Under earthquake excitation, a building structure at a specific site is subjected to complex seismic wavefields that in general consist of three translational and three rotational components of motion. However, it has been a significant challenge for scientists and engineers to understand and consider the complete 6-DOF motions in seismic performance assessments due to a lack of reliable measurements of rotational components of ground motion as well as the limitations inherent in various simplified methods to retrieve rotational motions from historically recorded translational motions. Recent advancements in High Performance Computing (HPC) and advanced software tools provide a new pathway to simulate 6-DOF earthquake motions with high-fidelity and high-frequency resolution. In this paper, a two-step computational workflow is proposed to consider 6-DOF earthquake ground motion input to building structures. This workflow is built upon the recently developed Earthquake Simulation (EQSIM) fault-to-structure framework that has been developed to fully utilize emerging GPU-based exascale computer platforms. The focus of this study is on the coupling of geophysics-based wave propagation models with engineering models of soil-structure systems through the Domain Reduction Method (DRM), a modular two-step algorithmic approach that allows complex three-dimensional, 6-DOF wavefields generated with the geophysics model to be appropriately introduced to drive the response of coupled soil-structure systems. As the first step, a geophysical model of a large domain of the earth, which simulates the earthquake source and propagation path effects, is developed and analyzed with the SW4 fourth order explicit wave propagation code to simulate complex earthquake waveforms. In the second step, an engineering model of a soil-building system with reduced dimensions is analyzed with implicit nonlinear finite element codes to evaluate the system response to complex incident seismic waves.

To begin, the two-step computational workflow was first verified by intercode comparison (OpenSees and ESSI vs SW4) under a simple source earthquake scenario, and subsequently, a more realistic earthquake scenario using an M_w 7.0 event. Nonlinear analyses were then performed of representative soil-building models in step two using the complex three-dimensional motions obtained from step one, which explicitly includes soil-structure interaction and rotational motions. For comparative purposes, a reference analysis was conducted for the same building models with traditional fixed-base conditions under pure translational motions. The preliminary analysis results indicate that the complex incident wavefields and SSI, can influence the response of buildings under the analyzed subdomains of the M_w 7.0 earthquake. This article describes the computational workflow and illustrates example applications. Further analysis will be required to assess the variability of these observations at more locations, softer soil conditions and with different earthquake magnitudes and rupture models.

Keywords: rotational motions; High Performance Computing; Domain Reduction Method; nonlinear analysis

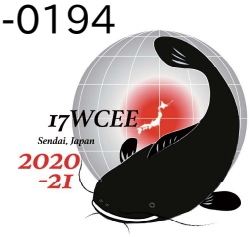

1. Introduction

The measurement of rotations of the ground surface during major earthquakes presents significant technical challenges and very few, if any, reliable rotation measurements appropriate for engineering building analysis exist. Lacking reliable recorded data, researchers have instead relied on a number of simplified methods with different assumptions and idealizations to estimate the rotational motions [1-5]. For example, measurement approaches based on a single station procedure [1] or a multiple station procedure such as geodetic methods [2], acceleration gradient methods [3] and surface distribution methods [4, 5] have been suggested. Previous studies based on these simple approaches have indicated that rotational motions can potentially contribute to structural response and can significantly increase the seismic demand on a building [4-9]. However, the rotational motions computed from these methods depend on measured translational and vertical records, which can be subject to significant limitations in frequency content, and in the near-field strong motion instruments can themselves be subjected to rotations, both of which make reliable retrival of displacement time histories used in rotation calculations problematic. For example, these records can miss important long-period components of ground displacements (including potential permanent ground displacements) that can occur in the near-fault region and instrument rotation effects on calculated displacements are indeterminant as instrument rotations are unmeasured. Consequently, rotational motions have not been considered for seismic performance assessment for building structures in current seismic design codes and standards. The influence of 6-DOF earthquake ground motions on building responses have yet to be comprehensively understood.

In view of the limitations inherent in the extraction of rotational motions from the historical records, seismologists and engineers can now utilize high-performance computing (HPC) and advanced software tools to simulate seismic waveforms and the associated six (three translational and three rotational) components of ground motions [10-12]. Recent advancements in HPC have permitted the simulation of regional-scale earthquake motions with high-fidelity and high-frequency resolution [10, 13, 14], providing a new pathway to explore the influence of the six components of earthquake ground motions on building responses. In this paper, a two-step computational workflow is proposed to consider 6-DOF motion input to building structures. This workflow is built upon the recently developed Earthquake Simulation (EQSIM) framework that is utilizing the U.S. Department of Energy's emerging GPU-based exascale computer platforms, as described by McCallen et al. [13, 14]. EQSIM is developing a multi-disciplinary fault-to-structure simulation workflow to couple geophysics codes and engineering codes in order to fully integrate earthquake hazards with seismic demands/risks of structures. This workflow is developed by coupling the regional-scale geophysics models for earthquake simulations with local engineering models of soil-structure systems through the Domain Reduction Method (DRM). This method, first proposed by Bielak et al. [15], is a modular two-step algorithm, which allows complex 6-DOF wavefields generated with a geophysics model to be appropriately introduced to drive the response of coupled soil-structure systems. To implement the EQSIM workflow, as the first step, a geophysical model of a large domain of the earth, which simulates the earthquake source and propagation path effects, is developed and analyzed with the SW4 fourth order wave propagation code [16] to simulate complex 3-D earthquake motions. In the second step, an engineering model of a soil-building system with reduced dimensions is developed and analyzed in two nonlinear, time-domain, finite element engineering codes: OpenSees [17] and ESSI [18]. To begin, an intercode comparsison was performed to evaluate the accuracy of the proposed workflow under a simple source earthquake scenario and subsequently, a representative M_w 7.0 earthquake scenario. Nonlinear analyses were then performed of representative soil-building models in step two using the 6-DOF motions obtained from step one, which explicitly includes soil-structure interaction and complex incident wavefields. For comparative purposes, a reference analysis was conducted for the same building models with traditional fixed-base conditions under pure translational motions. The influence of six components of motions on the building responses was then quantified by comparing these two analyses.

2. Verification of the computational workflow

In this section, the accuracy of the proposed two-step workflow is evaluated using a small-magnitude simple point source earthquake and a more realistic vertical strike-slip earthquake of M_w 7.0. Fig. 1 shows the

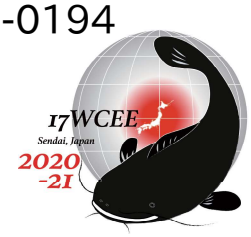

schematic workflow for the verification process. As seen in this figure, a regional-scale geophysics model is first developed in SW4 to simulate earthquake ground motions. A local model of reduced dimensions (hereafter referred to as DRM model) is developed in both OpenSees and ESSI with the same assumptions using the DRM theory to simulate a subdomain of the geophysics model. Ground motions of the subdomains of the geophysics model are then saved to drive the local DRM model. Comparison is made between the geophysics model and the DRM model at the same location in terms of the computed ground motions.

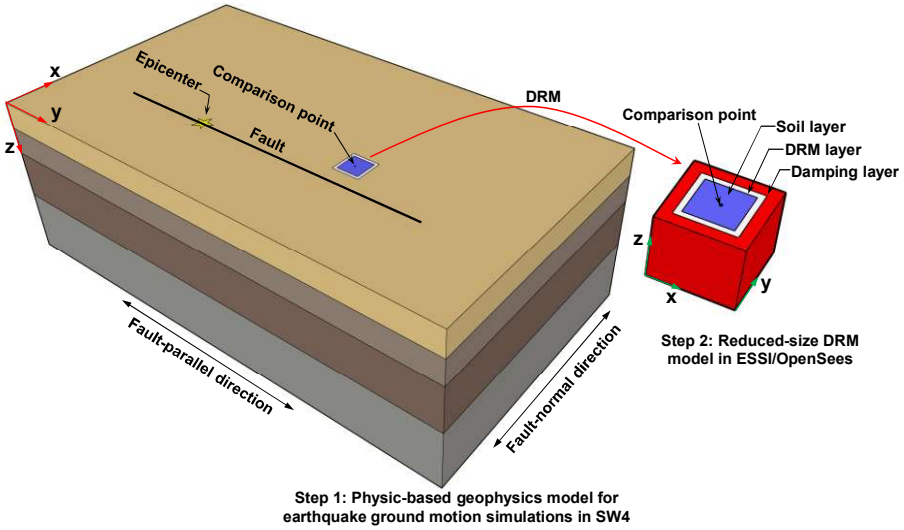

Fig. 1 - Schematic of the verification process of the two-step computational workflow

2.1 Earthquake scenarios

Two earthquake scenarios were simulated by regional-scale geophysics models in SW4: a simple double couple point source M_w=4.39 earthquake event with reverse fault (EQ1) and a M_w 7.0 vertical strike-slip earthquake event (EQ2). The former serves as a useful proof of concept, while the latter can produce representative, broad-band ground motions of high-fidelity and high-frequency resolution in the verification process.

The geophysics model included a 4 km × 7 km × 6 km domain to simulate the EQ1 with a simple double couple point source (reverse fault) and a Gaussian source time function. Mesh size was 10 m and Fig. 2a shows the plan view of the geophysics model and the subdomain of interest for the analysis. Motions of the subdomain A in Fig. 2a were saved for the analysis of subsequent local DRM models. The domain A was 200 m × 200 m × 200 m in dimensions with homogeneous material properties, including the compressional wave velocity V_p=1600 m/s, shear wave velocity V_s=800 m/s, mass density of soil ρ=2000 kg/m^2, quality factor of P-wave q_p=42.5, and quality factor of S-wave q_s=21.2.

For the M_w 7.0 earthquake scenario, the model was 40 km × 100 km × 30 km in order to accommodate a realistic rupture length (see Fig. 2b). The event was initiated at a depth of 9 km and ruptured to around 200 m below the surface. The minimum mesh size was 8 m in order to obtain earthquake motions with frequency resolution up to 5 Hz. The Graves and Pitarka (GP) kinematic rupture recipe [19] was used to generate the ruptures in this scenario. The GP rupture model permits the user to specify basic fault geometry and earthquake size and this information is used to generate low frequency (<1Hz) ground motions while sampling a von Karmen correlation function produces the high frequency motions [19]. This model contained a thin basin with a minimum V_s equal to 320 m/s. The materials of the basin varied along the depth were defined as follows.

$$V_p(d) = 1000 + 1.2d \quad (m/s) \tag{1}$$

$$V_s(d) = 320 + 19\sqrt{d} \quad (m/s) \tag{2}$$

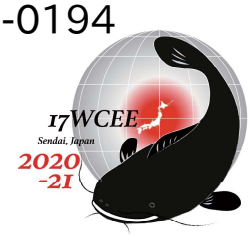

$$\rho(d) = 2140 + 0.125d \quad (kg/m^3) \tag{3}$$

$$q_p(d) = 128 \tag{4}$$

$$q_s(d) = 64 \tag{5}$$

where d is the depth of the soil layer. Motions of the subdomains in locations # 47, 53, 71, 83, 37 and 26, which are 1, 2, 5, 9, 16, and 24 km away from the fault, respectively, have been saved for the analyses of subsequent local DRM models (see Fig. 2b). Each domain was 200 m × 200 m × 200 m. All of them were located in the basin and had heterogenous material properties.

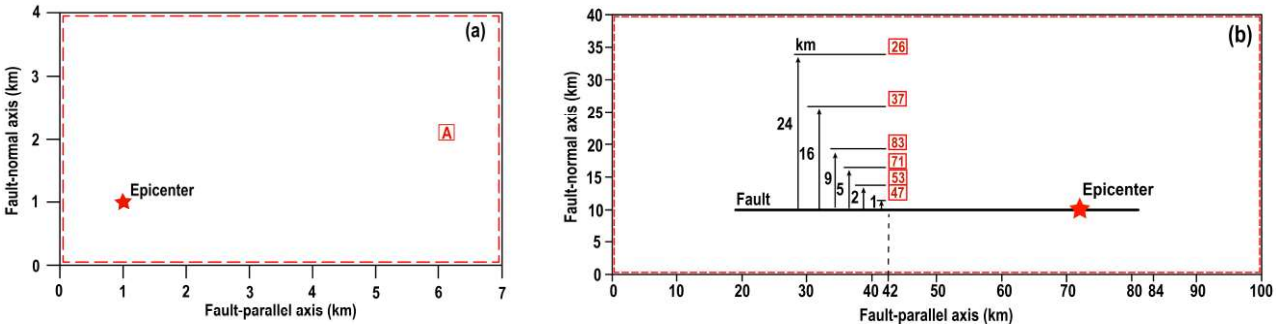

Fig. 2 – Plan view of the geophysics models for earthquake scenarios. (a) EQ1 and (b) EQ2

2.2 DRM model

The developed DRM model in both OpenSees and ESSI consists of a soil island for the interior region, a damping layer for the exterior region and a single-element layer between these two regions for the DRM layer, as seen in Fig. 3. In this modeling structure, the complex seismic waves (displacements and accelerations) from the geophysics model are input at the DRM layer, and automatically converted to equivalent forces in OpenSees and ESSI based on the equations in Bielak et al. [15]. The damping layer is to appropriately simulate the absorbing boundary to eliminate spurious waves caused by the reflection of waves back into the soil island.

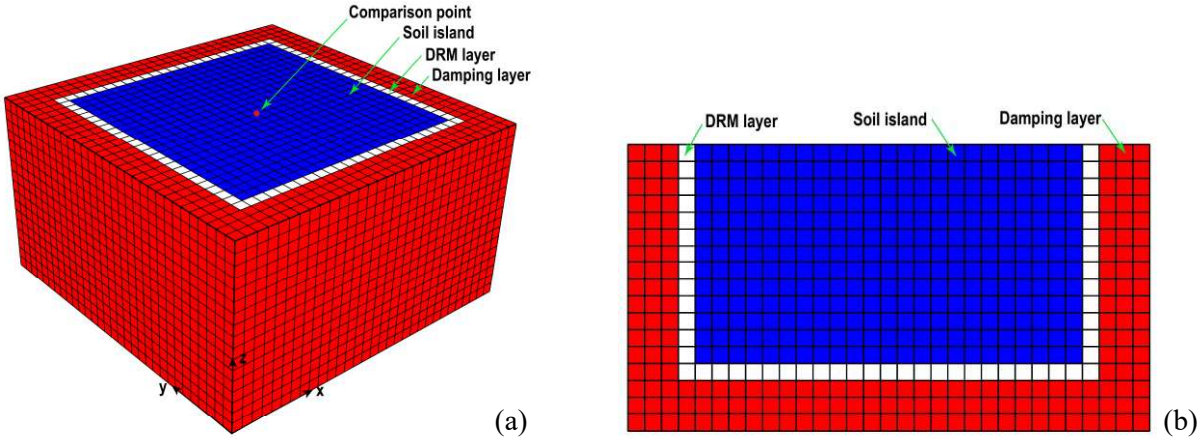

Fig. 3 – DRM model in OpenSees and ESSI. (a) 3D view and (b) elevation view

Two 3D DRM models were developed respectively in OpenSees and ESSI with the same assumptions. Fig. 3 illustrates the developed DRM models. Model 1 was to simulate the subdomain A of the geophysics model for EQ1 (see Fig. 2a) while Model 2 was to simulate the subdomain #53 of the geophysics model for EQ2 (see Fig. 2b). In model 1, the soil island had dimensions of 100 m × 100 m × 100 m and the mesh size was constant at 10 m. In model 2, the soil island had dimensions of 184 m × 184 m × 104 m and the mesh size was constant at 8 m. Both models had three layers of elements for the damping layer. 8-node brick elements

with elastic materials were used to simulate all components of the DRM model. The boundary conditions were set up in such a way that all nodes of the exterior surfaces of the damping layer excluding the top surface were fixed in all degrees of freedom.

For the purpose of verification, the material properties of DRM models in OpenSees and ESSI were set the same as those of subdomains of interest in the geophysics model. The soil properties of the geophysics model were converted to equivalent elastic material properties based on the following equations [20-21].

$$G = \rho v_s^2 \tag{6}$$

$$E = 2(1+\mu)G \tag{7}$$

$$\mu = \frac{V_p^2 - 2V_s^2}{2(V_p^2 - V_s^2)} \tag{8}$$

where G and E are the shear and elastic modulus of the soil at small strain, respectively and μ is the Poinsson's ratio. Based on these equations, the equivalent elastic material properties along the depth of the DRM models were computed for the subdomains of interest of the analyzed earthquake events, which were then assigned to the 8-node brick elements.

In the DRM models, Rayleigh damping was used to represent the energy dissipation. In order to achieve equivalent energy dissipation with the geophysics models, the equivalent damping ratio of the soil island and damping layer of the DRM models was computed based on the Eq. (9) [22].

$$\xi = \frac{1}{2q_s} \tag{9}$$

To achieve constant damping ratio for a wide range of frequencies, the two periods used to anchor the average equivalent damping ratio were set at 1.0 s and 0.1 s. For the damping layer, a large damping ratio (e.g. 50%) was used to appropriately simulate energy absorbing at the exterior boundary.

The input motions (displacements and accelerations) of the DRM models were converted from the output motions (velocities) of the subdomains of interest in the geophysics model by a multi-step conversion procedure outlined in Fig. 4.

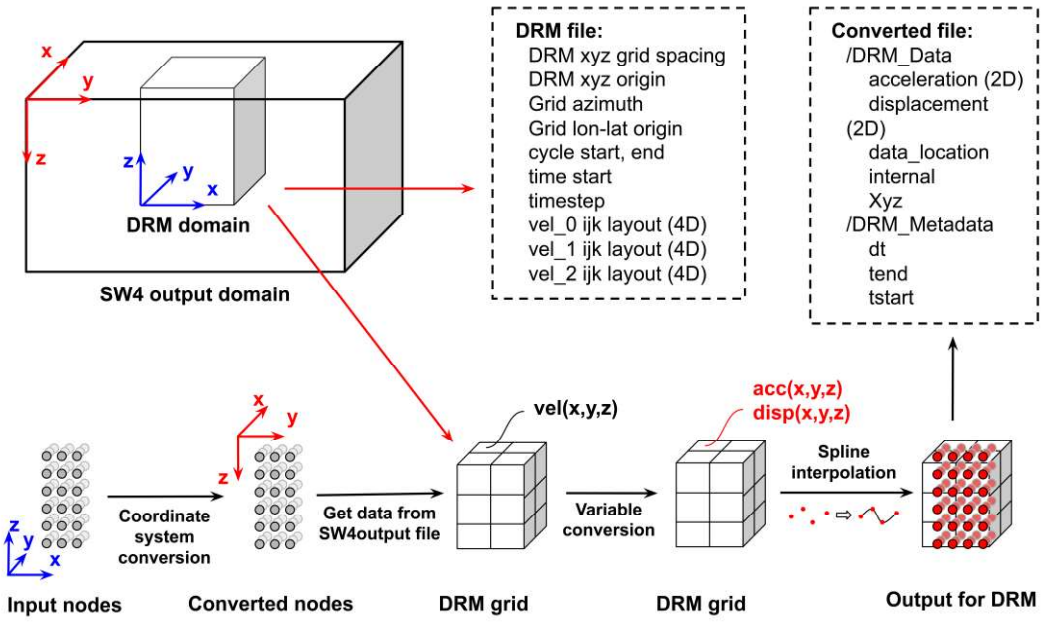

Fig. 4 - A multi-step motion conversion procedure to generate the input motions for the DRM models.

Step 1: Translate the global coordinate system of the local engineering system model into the global coordinate system of the SW4 regional geophysics model with appropriate coordinate system orientation and global x, y, z locations.

Step 2: Develop a min/max bounding box surrounding the domain of the local engineering system model and convert the velocities of the nodes within this box to accelerations and displacements.

Step 3: Interpolate the data at the grid point of SW4 model to continuous acceleration and displacement fields using spline-function, on which the grid point accelerations and displacements on the DRM boundary of the local engineering model are then determined.

2.3 Comparison of motions between the geophysics and DRM models

Comparison was made of the computed motions at a comparison point (see Fig. 3a) in three translational directions between the geophysics model in SW4 and the DRM models in OpenSees and ESSI. In addition, the surface rotational motions about the fault-normal (FN) and fault-parallel (FP) axes were also computed and compared. Fig. 5 shows the comparison of surface translational motions for a simple source earthquake. Fig. 6 shows the comparison of surface rotational motions for the simple source earthquake.

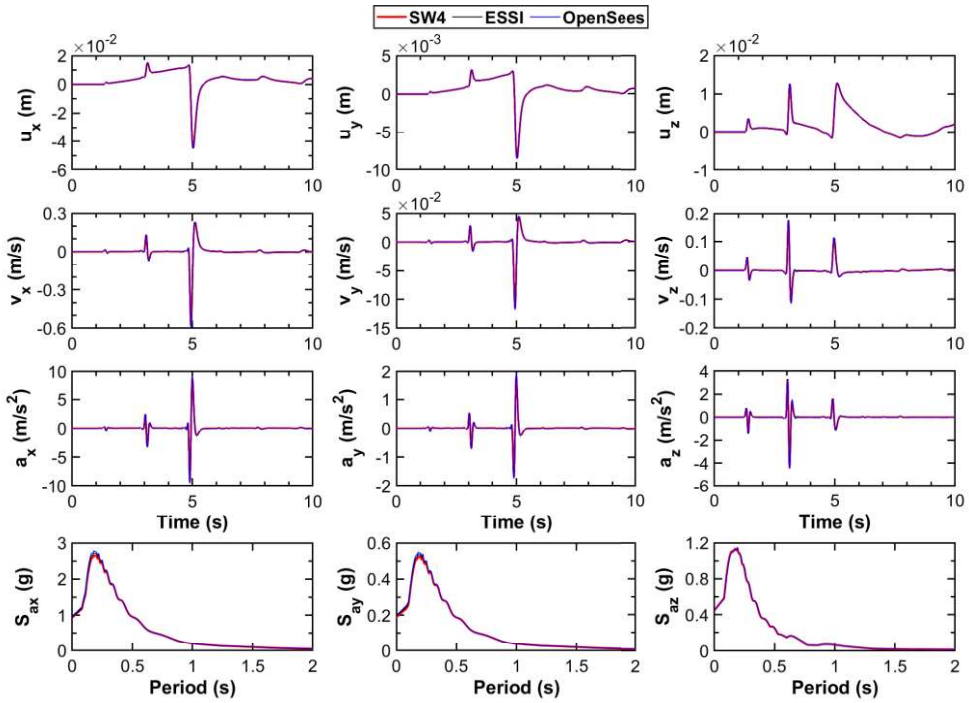

Fig. 5 - Comparison of surface translational motions at domain A for the simple source earthquake.

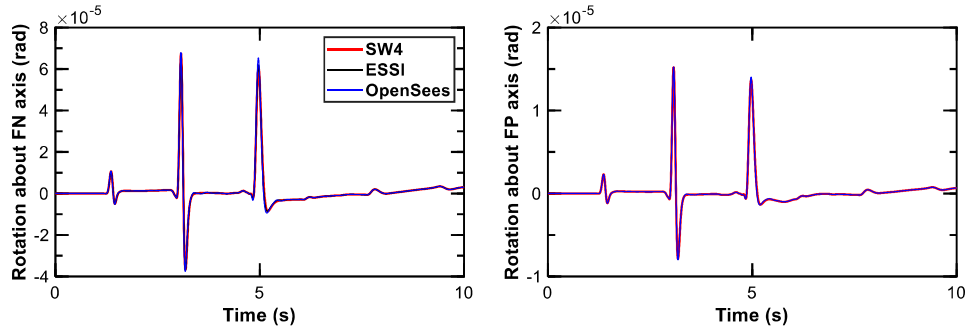

Fig. 6 - Comparison of rotational motions at domain A of the simple source earthquake.

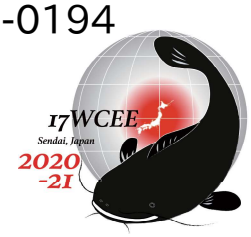

As shown in Fig. 5, exceptionally good agreement is obtained for the comparison of the surface translational motions between the geophysics model and the DRM models for the simple source earthquake, including displacement, velocity and acceleration histories in terms of transient waveforms and amplitudes. Good agreement is also obtained for the comparison of the rotational motions about FN and FP axes in Fig. 6. These observations indicate that the proposed workflow can work effectively and efficiently in reproducing complex three-dimensional earthquake ground motions including the rotational motions and hence can be used to investigate the influence of six components of earthquake ground motions on nonlinear building responses.

Figs. 7 and 8 show the comparison of surface translational and rotational motions of subdomain 53 for the M_w 7.0 earthquake, respectively. As seen in these two figures, excellent agreement is also obtained for the comparison of computed translational motions and rotational motions between the geophysics model and the DRM models under the M_w 7.0 earthquake. These provide confidence in the DRM models to reproduce the representative broadband ground motions and again confirm the accuracy of the proposed workflow. It is noted that the peak ground rotations obtained from this rupture scenario are on the order of 10^{-4}~10^{-3} rad, which fall into the typical 10^{-6}~10^{-3} rad range from very limited data measured in the near-fault region [23].

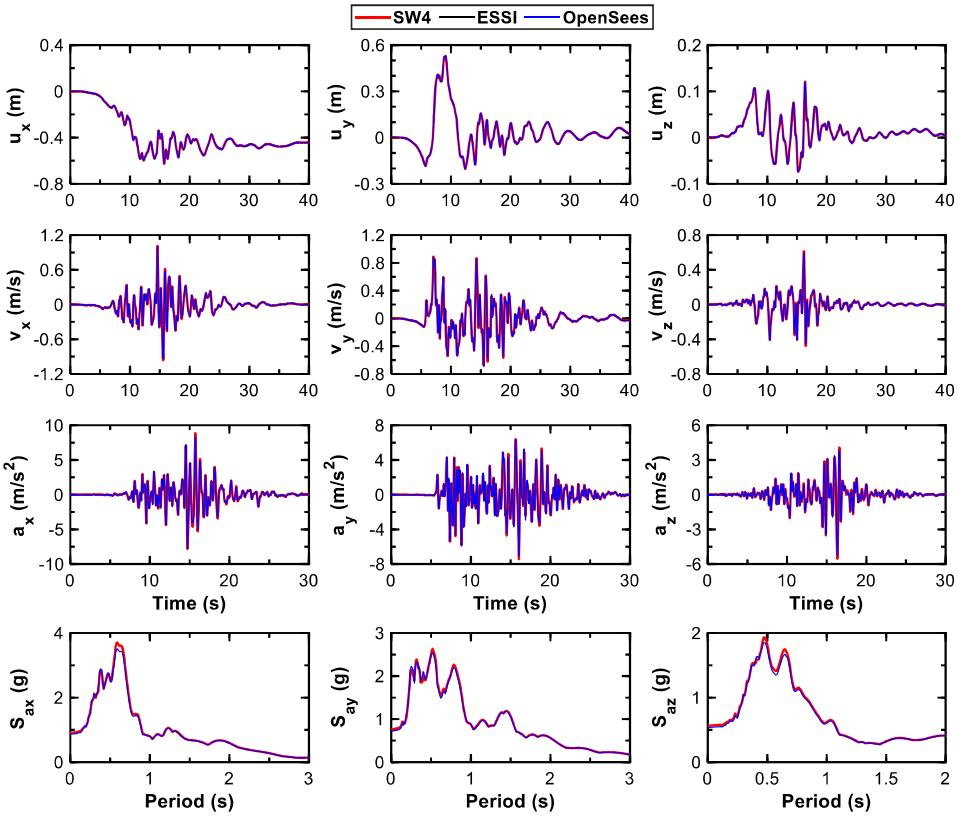

Fig. 7 - Comparison of surface translational motions at subdomain 53 of the M_w 7.0 earthquake.

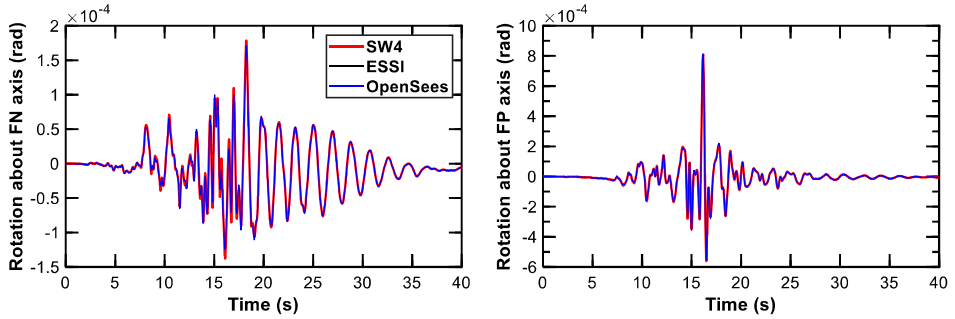

Fig. 8 - Comparison of rotational motions at subdomain 53 of the M_w 7.0 earthquake.

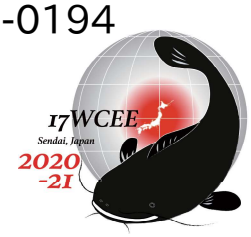

3. Influence of rotational motions on building responses

With the confidence built in the workflow, representative steel moment-resisting frame buildings were then included in the local DRM models to study the influence of complex incident wavefields on the nonlinear building responses, as seen in Fig. 9. For this purpose, four typical steel moment-resisting frame buildings of 3-, 9-, 20- and 40-story were employed. The broadband ground motions from the representative M_w 7.0 earthquake scenario in EQ2 were used in the first step. In the second step, the building models with two different boundaries were analyzed. In case 1, the building models were simulated with the DRM boundary, where the buildings were supported by spread foundations, which were then embedded inside the soil. The complex wavefields generated from the remote earthquake in step 1 were applied at the DRM layer to drive the DRM models of soil-structure systems. This case allows the consideration of complex wavefields including rotational motions and soil-structure interaction (SSI). The case 2 was worked as a reference where the building models were simulated with fixed base conditions under uniform translational and vertical excitations. This case represents the conventional building analysis where incident motions are assumed to be due to pure vertically propagating shear (for transverse motions) and compressional (for vertical motion) waves.

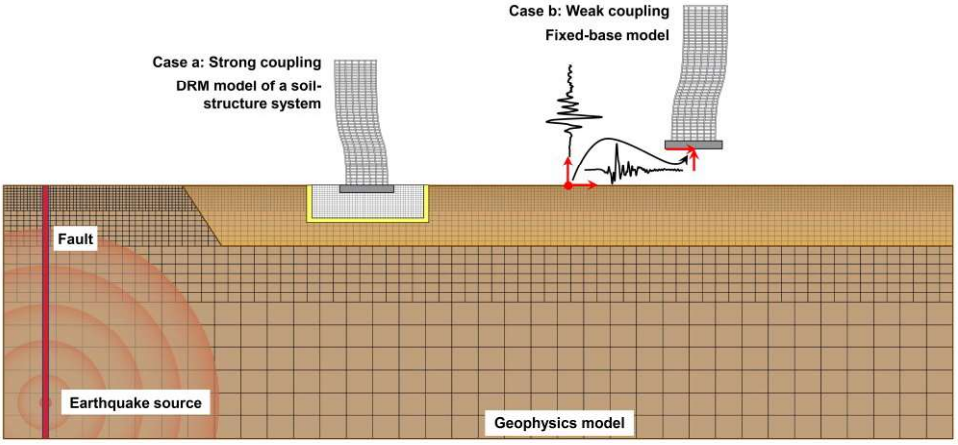

Fig. 9 - DRM to couple earthquake motion simulations with seismic risk assessment of buildings.

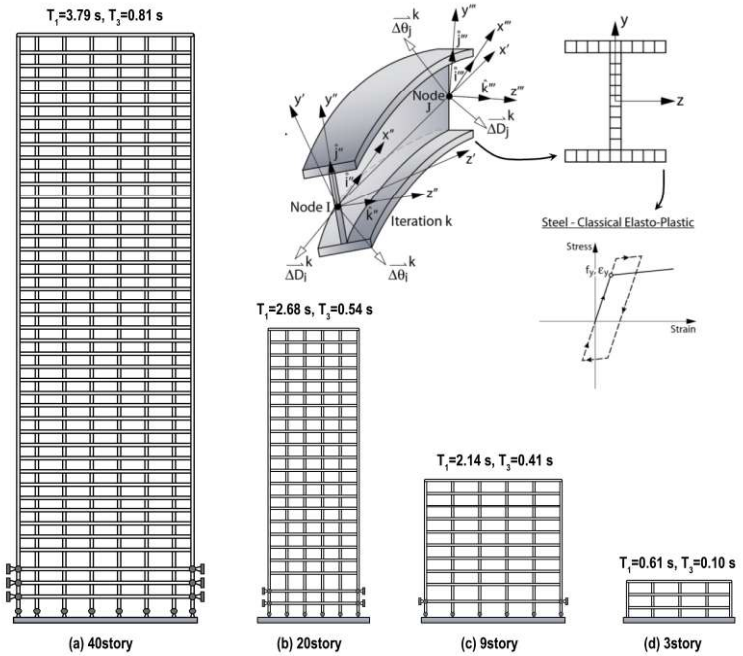

Fig. 10 - Fixed-base models of the four canonical steel moment-frame buildings in OpenSees and ESSI.

Fig. 10 shows the developed fixed-base models of the four building models in the OpenSees and ESSI codes. These buildings are simulated as planar models with a fiber-based cross section and classical plasticity with kinematic hardening to represent nonlinear material behavior. The modeling details of these buildings are referred to Wu et al. [24]. These models have fundamental periods ranging from 0.61s to 3.78s, which is representative of buildings from low to high heights.

Only the in-plane excitations were used to drive the cases 1 and 2 models due to the 2D simplification of modeling. Nonlinear response history analyses were performed in the six subdomains of interest of the EQ2 (see Fig. 2b). For each domain, the models were analyzed in both FN and FP directions. The peak inter-story drift (maximum absolute relative displacement between two adjacent floors, ID) of each story was then output. In order to evaluate the influence of complex incident waves and SSI, a parameter β is defined as Eq. (10) to quantify the difference of peak ID of each story between case 1 and case 2.

$$\beta_i = \frac{Max\ |ID|_{i\_DRM} - Max\ |ID|_{i\_fix}}{Max\ |ID|_{i\_fix}} \tag{10}$$

where i represent the story number and the subscript *DRM* and *fix* represent the DRM and fixed-base models, respectively. The β was then computed for each model and domain. Figs. 11a and 11b show the distribution of β along the building height for all buildings in the FN and FP directions of the six domains, respectively.

As seen in Fig. 11a, among the six domains in FN direction, the difference β varies from -3.1% to 11.9% for the 3-story model, from -5.9% to 7.8% for the 9-story model, from -17.8% to 10.1% for the 20-story model and from -14.0% to 9.2% for the 40-story model. While among the six analyzed domains in FP direction (see Fig. 11b), the difference β varies from -10.3% to 9.3% for the 3-story model, from -11.2% to 10.7% for the 9-story model, from -13.2% to 10.6% for the 20-story model and from -9.2% to 7.9% for the 40-story model. It is interesting to note that the variation of difference of β is within the range of ±20% for all buildings. This is mainly attributed to the relatively stiff soil supporting the buildings. Based on Stewart et al. [25], the single most important parameter controlling the significance of inertial interaction is $h/(V_sT)$ and the inertial SSI effects are generally negligible for $h/(V_sT)<0.1$, where h is the total height of the buildings. In this study, the parameter $h/(V_sT)$ is 0.06, 0.05, 0.09, and 0.13 for the 3-, 9-, 20- and 40-story buildings, respectively, which is either less or close to the limit 0.1. To explore more comprehensively the effects of complex incident wavefields and SSI on the nonlinear response of buildings, further studies on the spatial variability of rotational motions, lower soil stiffness and building structural types are required.

In summary, the complex seismic incident wavefields and SSI can have an influence on the responses of buildings under the six domains of the M_w 7.0 earthquake. The overestimation or underestimation depends on the locations of the analyzed domains, i.e. motion characteristics of these domains and dynamic characteristics of building models. These results are far from complete since the analysis is only performed at six different locations of the large-scale geophysics model with FN and FP motions. Further analysis is required to assess the variability of these observations at more locations, softer soil conditions, different earthquake magnitudes and sources, and different types of buildings, for example stiffer shear wall buildings and braced frames versus the flexible moment frames utilized in the current analysis.

4. Conclusions

In this study, a two-step computational workflow has been implemented in an HPC framework to include the complete 6-DOF earthquake ground motions in seismic analysis of building structures by coupling of regional geophysics models for earthquake ground motion simulations with local engineering models of soil-structure systems. The coupling is obtained through the Domain Reduction Method (DRM), a two-step algorithmic approach that allows complex three-dimensional, 6-DOF complex wavefields generated with a geophysics model to be appropriately introduced to drive the response of coupled soil-structure systems. In order to implement the computational workflow, in step 1, a regional-scale geophysics model, which explicitly considers earthquake source and wave propagation, is simulated and analyzed for earthquake ground motions of high frequency resolution and high-fidelity in the four-order finite difference code SW4. In step 2, a local

engineering model of a soil-structure system is developed respectively in two time-domain, finite element nonlinear codes OpenSees and ESSI to represent a subdomain of the step 1 model without modeling of earthquake source and wave propagation.

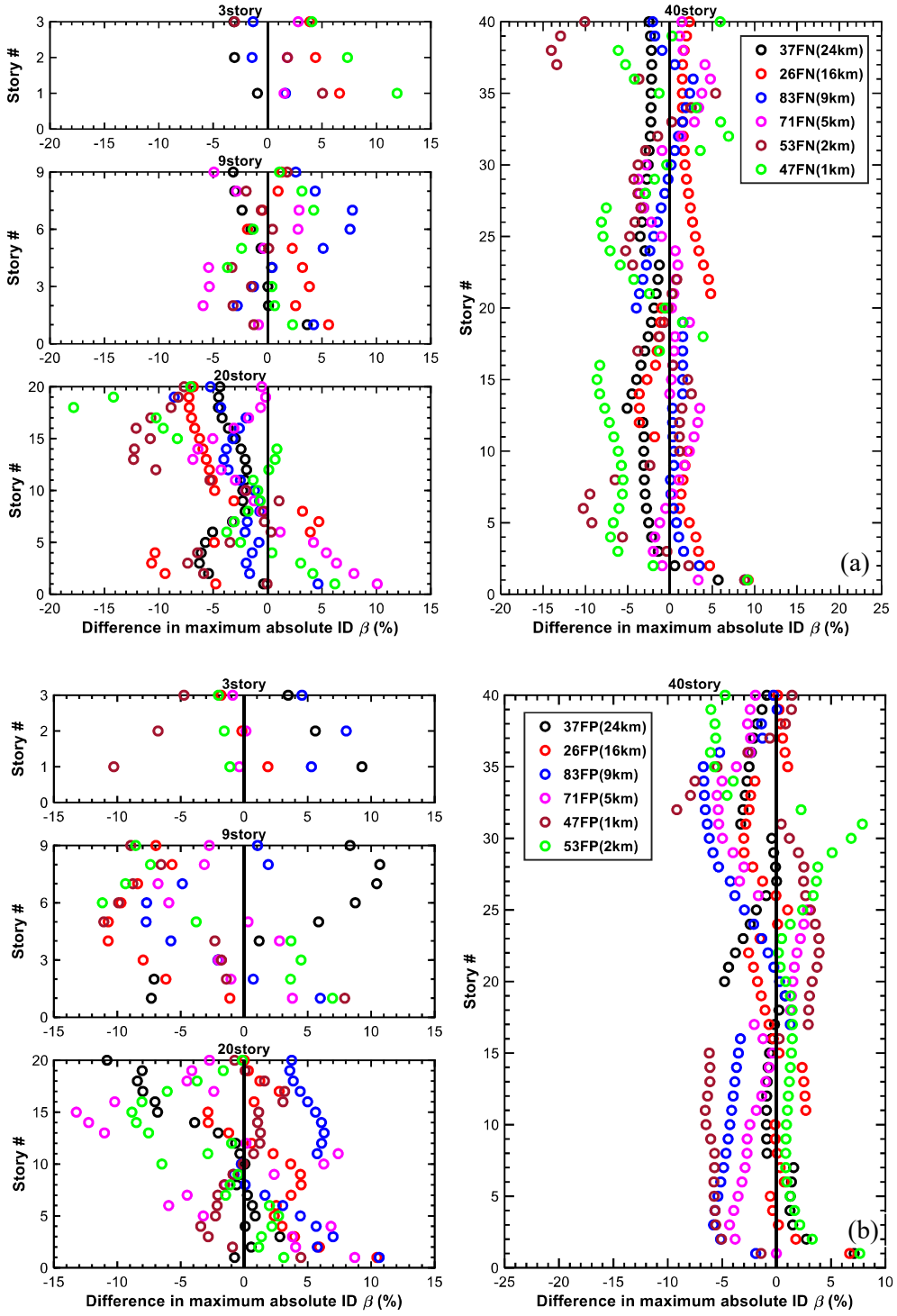

Fig. 11 - Difference in peak ID of each story β between the DRM and fixed-base models at the six domains of EQ2. (a) FN components and (b) FP components

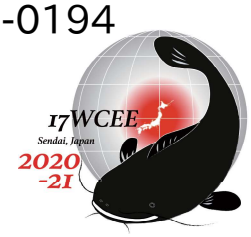

To begin, the accuracy of the two-step computational workflow was demonstrated by inter-code comparison with simple waveform motions from a simple source earthquake and more representative broadband motions from a M_w 7.0 vertical strike-slip earthquake. Excellent agreement was obtained for the comparison of computed translational motions as well as rotational motions between the regional-scale geophysics model and the local engineering models for both earthquakes. This provides confidence in the accuracy of the proposed workflow in reproducing the complex 6-DOF components of earthquake ground motions. This type of simulation provides a methodology to evaluate the influence of 6-DOF motions (i.e. complex seismic wavefields) on the nonlinear responses of buildings with representative, high-frequency resolution synthetic motions rather than the rotational motions extracted from historical records.

Local soil-structure systems were then simulated with the workflow by introducing four representative steel moment resisting frame buildings into the local engineering models. For comparative purpose, the building models were also analyzed with the conventional fixed-base conditions under pure translational and vertical motions. The preliminary analysis results indicate that the complex incident wavefields and SSI can have an influence on the inter-story drift of all four building models under the analyzed subdomains of the M_w 7.0 earthquake. These results are far from complete since the analysis has only been performed for a limited set of locations and limited ruptures models in the large-scale geophysics model with FN and FP motions. With the computational framework developed and implemented in an HPC ecosystem, further analysis will be performed to fully assess the variability of these observations at more locations, for softer soil deposits and for different earthquake magnitudes and sources.

5. Acknowledgements

This research was supported by the Exascale Computing Project (ECP), Project Number: 17-SC-20-SC, a collaborative effort of two U.S. Department of Energy (DOE) organizations - the Office of Science and the National Nuclear Security Administration. The simulations described utilized computing resources of the National Energy Research Scientific Computing Center (NERSC) at Lawrence Berkeley National Laboratory, a DOE Office of Science User Facility operated under Contract No. DE-AC02-05CH11231. The authors appreciate the assistance of Dr. Arben Pitarka of Lawrence Livermore National Laboratory in the development of representative fault rupture models. Special recognition is given to Houjun Tang of Lawrence Berkeley National Laboratory for his assistance in converting the SW4 output motions to the input motions of local engineering models in OpenSees and ESSI.

6. References

[1] Basu D, Whittaker AS, Constantinou MC (2012): Estimating rotational components of ground motion using data recorded at a single station. *Journal of Engineering Mechanics*, **138** (9),1141–1156.

[2] Spudich P, Steck LK, Hellweg M, Fletcher JB, Baker L (1995): Transient stress at Parkfield California, produced by the M 7.4 Landers earthquake of June 28, 1992: Observations from the UPSAR dense seismography array. *Journal of Geophysical Research*, **100**, 675-690.

[3] Basu D, Whittaker AA, Constantinou MC (2013): Extracting rotational components of earthquake ground motion using data recorded at multiple stations." *Earthquake Engineering & Structural Dynamics*, **42**, 451-468.

[4] Basu D, Whittaker AA, Constantinou MC (2015): Characterizing rotational components of earthquake ground motion using a surface distribution method and response of sample structures. *Engineering Structures*, **99**, 685-707.

[5] Basu D, Whittaker AS, Constantinou MC (2012): Characterizing the rotational components of earthquake ground motion. *MCEER-12-0005 Technical Report*, MCEER, State University of New York at Buffalo, New York.

[6] Bycroft GN (1980): Soil-foundation interaction and differential ground motions. *Earthquake Engineering & Structural Dynamics*, **8**, 397-404.

[7] Zembaty Z (2009): Rotational seismic code definition in Eurocode 8, Part 6, for slender tower-shaped structures. *Bulletin of the Seismological Society of America*, **99** (2B), 1483-5.

[8] Trifunac MD (2009): Review: rotation in structural response." *Bulletin of the Seismological Society of America*, **99** (2B), 968-979.

[9] Trifunac MD (2009): The role of strong motion rotations in the response of structures near earthquake faults. *Soil Dynamics and Earthquake Engineering*, **29**, 382-393.

[10] Johansen H, Rodgers A, Petersson NA, McCallen D, Sjogreen B, Miah M (2017): Toward exascale earthquake ground motion simulations for near-fault engineering analysis. *Computing in Science and Engineering*, **19** (5), 27-37.

[11] Rodgers A, Petersson NA, Pitarka A, McCallen D, Sjogreen B, Abrahamson N (2018): Broadband (0-5Hz) fully deterministic ground-motion simulations of a magnitude 7.0 Hayward fault earthquake: comparison with empirical ground-motion models and 3D path and site effects from source normalized intensities. *Seismological Research Letters*, **90** (3), 1268-1284.

[12] McCallen D, Petersson NA, Rodgers A, Miah M, Pitarka A, Petrone F, Tang H (2020): The earthquake simulation (EQSIM) framework for physics-based fault-to-structure simulations. *17th World Conference on Earthquake Engineering*, September 13 to 18.

[13] McCallen D, Petersson A, Rodgers A, Pitarka A, Miah M, Petrone F, Sjogreen B, Abrahamson N, Tang H (2020): EQSIM–A multidisciplinary framework for fault-to-structure earthquake simulations on exascale computers, part I: Computational models and workflow. *Earthquake Spectra*, doi:10.1177/8755293020970982.

[14] McCallen D, Petrone F, Miah M, Pitarka A, Rodgers A, Abrahamson N (2020): EQSIM–A multidisciplinary framework for fault-to-structure earthquake simulations on exascale computers, part II: Regional simulations of building response. *Earthquake Spectra*, doi:10.1177/8755293020970980.

[15] Bielak J, Loukakis K, Hisada Y, Yoshimura C (2003): Domain reduction method for three-dimensional earthquake modeling in localized regions, part I: theory. *Bulletin of the Seismological Society of America*, **93** (2), 817-824.

[16] Petersson NA, Sjogreen B (2012): Stable and efficient modeling of anelastic attenuation in seismic wave propagation. *Communications in Computational Physics*, **12** (1), 193-225.

[17] McKenna F, Scott M, Fenves G (2010): Nonlinear finite-element analysis software architecture using object composition. *Journal of Computing in Civil Engineering*, **24** (1), 95-107.

[18] Jeremic B, Jie G, Cheng Z, Tafazzoli N, Tasiopoulou P, Pisano F, Abell J, Watanabe K, Feng Y, Sinha K, Behbehani F, Yang H, Wang H (2020): The Real-ESSI Simulator System. University of California, Davis. http://sokocalo.engr.ucdavis.edu/~jeremic/Real_ESSI_Simulator/.

[19] Graves R, Pitarka A (2014): Refinements to graves and pitarka (2010) broadband ground motion simulation method. *Seismological Research Letters*, **86** (1), 75-80.

[20] Olsen KB, Day SM, Minster JB, Cui Y, Chourasia A, Okaya DA, Maechling PJ, Jordan, TH (2008): TeraShake2: simulation of Mw7.7 earthquakes on the southern San Andreas Fault with spontaneous rupture description. *Bulletin Seismological Society of America*, **98**, 1162-1185.

[21] Sas W, Gabrys K, Sobol E, Szymanski A (2016): Dynamic characterization of cohesive material based on wave velocity measurements. *Applied Sciences*, **6** (2), 49.

[22] Semblat JF (1997): Rheological interpretation of Rayleigh damping. *Journal of Sound and Vibration*, **206** (5), 741-744.

[23] Trifunac MD (2009): Review: rotations in structural response. *Bulletin of the Seismological Society of America*, **99** (2B), 968-979.

[24] Wu S, Eckert E, Huang J, McCallen D (2020): Evaluation of the Domain Reduction Method applied to broad-band, near-fault ground motions with inter-code comparisons. *Report No. CCEER-20-08*, Center for Civil Engineering Earthquake Research, Department of Civil and Environmental Engineering, University of Nevada, Reno, NV.

[25] Stewart J, Crouse C, Hutchinson TC, Lizundia B, Naeim F, Ostadan F (2012): Soil-structure interaction for building structures. National Institute of Standards and Technology and NEHRP Consultants Joint Venture.

